International Journal of Remote Sensing
Vol. 34, No. 8, 20 April 2013, 2969–2982

Taylor & Francis
Taylor & Francis Group

InSAR time-series analysis of land subsidence in Bangkok, Thailand

Anuphao Aobpaet[a]*, Miguel Caro Cuenca[b], Andrew Hooper[b], and Itthi Trisirisatayawong[a]

[a]*Survey Engineering, Chulalongkorn University, 10330 Bangkok, Thailand;* [b]*Geoscience & Remote Sensing, Delft University of Technology, 2628 CN Delft, The Netherlands*

(*Received 2 July 2011; accepted 16 September 2012*)

Land subsidence poses a serious risk to the low-lying coastal city of Bangkok, Thailand; major flooding occurred there in 1983 and again in 2011. Extreme water pumping in the past led to subsidence rates of up to 120 mm year^{-1}. Although water extraction is now controlled, maximum rates measured by levelling today are still up to 20 mm year^{-1}. In this study, we apply interferometric synthetic aperture radar (InSAR) time-series analysis to study subsidence in Bangkok between October 2005 and March 2010. We validate the InSAR results, by comparing levelling rates and find good agreement between the two techniques. We detect approximately 300,000 coherent pixels overall, with an average density of 120 observations per km^2. This is two orders of magnitude greater than the density of levelling benchmarks and reveals subsiding areas that are missed by the levelling network.

Downloaded by [anuphao aobpaet] at 17:59 21 January 2013

1. Introduction

The province of Bangkok, Thailand, is under a continuous threat of flooding. This region has a very low elevation, with heights ranging from 0.5 to 1.50 m above mean sea level, and is situated on a river delta (Figure 1). The area has already suffered from major floods in 1983 and 2011. Monitoring of subsidence in Bangkok is therefore crucial, particularly as the city of Bangkok is the most populated metropolitan area of Thailand and is the economic and political heart of the country. Subsidence in Bangkok and the surrounding areas was first detected in the late 1960s and early 1970s (Haley and Aldrich 1970; Brand and Paveenchana 1971; Edward 1976). However, surface subsidence was not measured quantitatively until 1978 (Nutalaya 1981). Monitoring of land subsidence has been performed since then using levelling. Levelling benchmarks were installed in the late 1970s by Thai authorities, and they have been maintained since then by the Royal Thai Survey Department (RTSD), which has also performed annual campaigns since 1978. Details of the levelling network can be found in Bontebal (2001).

Levelling surveys revealed very high subsidence rates of up to 120 mm year^{-1} from 1978 to 1981. Bontebal (2001) and Phien-wej et al. (2006) reported a decrease in the rates for later periods with values of around 35 mm year^{-1} in 1985–1988 and to 30 mm year^{-1} in 1988–1991 (Ramnarong 1983; Yong, Maathuis, and Turcott 1995; Ramnarong et al. 1998). The reduction in subsidence rates was caused by new laws, which were introduced in the late 1980s to decrease groundwater pumping. The maximum subsidence occurred around

*Corresponding author. Email: anuphao@eoc.gistda.or.th

ISSN 0143-1161 print/ISSN 1366-5901 online
© 2013 Taylor & Francis
http://dx.doi.org/10.1080/01431161.2012.756596
http://www.tandfonline.com

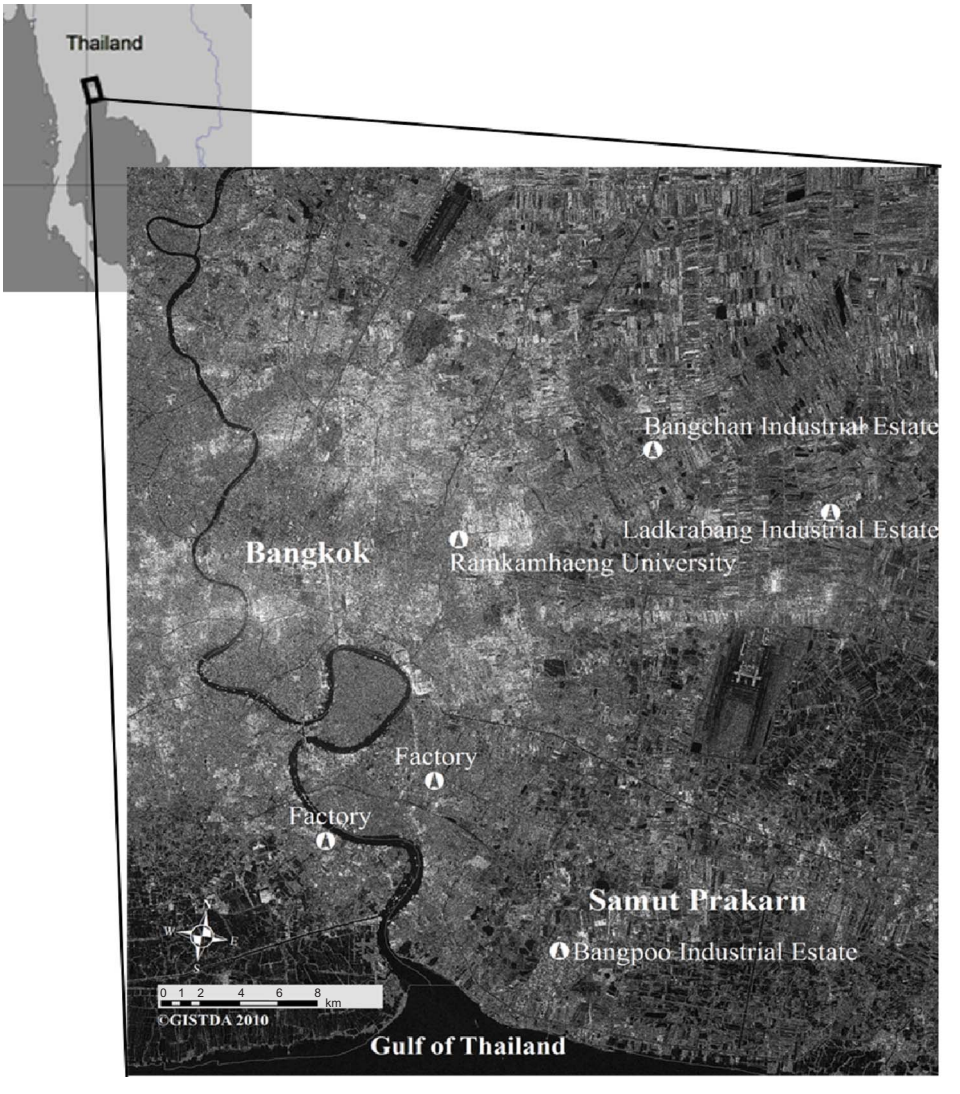

Figure 1. Locations of the past maximum subsidence area (Ramkhamhaeng University, Bang Kapi) and the industrial estate growth in the east and south of Bangkok.

Ramkhamhaeng University in the Bang Kapi district and the new industrial area in the eastern part of Bangkok (locations shown in Figure 1). The total subsidence measured in these areas reached maximum values of 950 mm between 1978 and 2000.

The most recent levelling results show maximum rates of 20 mm year^{-1} inside Bangkok (RTSD, personal communication, 2010). However, the levelling network is rather sparse, and interpolated maps may underestimate the rates between benchmarks. The geological setting of Bangkok further complicates the study of subsidence from levelling data. Features such as roads, pavement, and walkways lie on the soft clay ground surface, while most buildings and bridges rest on piles standing on the deeper and less compressible sand layer 20–50 m beneath the surface. As a result of differing water content and physical properties, the subsidence rates of the soft clay layers are faster than those of the sand layer. This

Downloaded by [anuphao aobpaet] at 17:59 21 January 2013

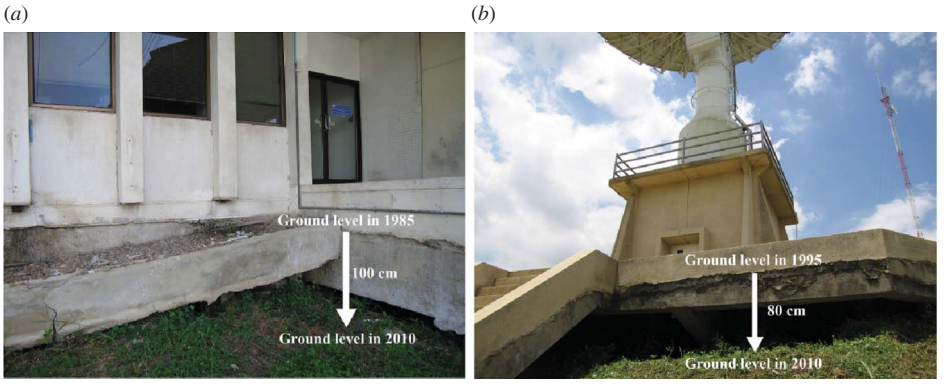

Figure 2. Gaps opened due to differences between subsidence of the ground surface and buildings whose foundations rest on the sand layer.

Downloaded by [anuphao aobpaet] at 17:59 21 January 2013

effect is shown in Figures 2(*a*) and (*b*), where the ground appears to subside faster than the buildings. The same situation can be found in other parts of the city. Most levelling monuments are metal plates fixed to bridges and public buildings. Ground monuments do exist, but they are usually destroyed or moved in a short time due to development and construction. As such, levelling data provide mainly subsidence rates of the sand layer, not those of the ground surface. These estimates are, however, of great value for many applications such as drainage and flood protection.

In contrast with the sparsity of the levelling network, interferometric synthetic aperture radar (InSAR) time-series analysis can provide a network of observations with a density of 100 observations per km^2 or more for urban areas. The precision of InSAR time-series techniques can be up to 1 mm $year^{-1}$ (Marinkovic et al. 2008). These techniques use a set of synthetic aperture radar (SAR) images to estimate topography and surface motion.

Conventional InSAR, which uses pairs of SAR images (see e.g. Goldstein and Zebker 1987; Hanssen 2001), has also been applied to the Bangkok metropolitan area; Kuehn et al. (2004) reported that the maximum subsidence rate was 30 mm $year^{-1}$ in the southeast and southwest alongside the Chao Phraya River during the time span of February 1996 to October 1996. However, this result may not reflect accurately the actual deformation rates, because of the short time span and limited number of images used. Our contribution focuses on applying InSAR time-series analysis to study subsidence in Bangkok and assessing the potential of the technique for subsidence monitoring in this area. Time-series analysis methods, namely persistent scatterer interferometry (PSI) (Ferretti, Prati, and Rocca 2001; Hooper, Segall, and Zebker 2007) and small baseline (SB) techniques (Berardino et al. 2002; Fornaro, Pauciullo, and Serafino 2009), were developed to address the limitations of differential InSAR such as atmospheric delay and loss of coherence.

With InSAR time-series analysis, the phase evolution of pixels is used to detect those that remain coherent within the time span covered by the data set. As a result, it is possible to detect and measure millimetre variations in the satellite's line-of-site (Perissin 2008). Worawattanamateekul (2006) applied the PSI technique for deformation estimation in Bangkok using data acquired by the European Remote Sensing satellites, ERS-1 and ERS-2, which covered the time period of 1992–2000. However, the algorithm to detect stable scatters used by Worawattanamateekul (2006) was not optimal for the limited number of images, resulting in relatively large errors of 6–8 mm $year^{-1}$. In this contribution, we apply the Stanford Method for Persistent Scatterers (StaMPS) algorithm (Hooper, Segall, and Zebker 2007) combined with a SB approach (Hooper 2008). These algorithms can

produce reasonable results, even for a small number of images (Hooper, Segall, and Zebker 2007).

2. Data description

We employ 19 RADARSAT-1 images in F1N beam mode with nominal azimuth resolution of 8.9 m and nominal range resolution of 6.0 m in the slant range. The images cover an area of approximately 2500 km^2 centred in Bangkok (13° 33′ 44.37″ N, 100° 38′ 47.76″ E).

The images were acquired between October 2005 and March 2010 in ascending orbit (Path-Row: 2–60). From the available radar images, the fine beam mode is the best spatial resolution available for the RADARSAT-1 system. Each original fine beam position can either be shifted closer to or further away from nadir by modifying timing parameters and adding 10 new positions with offset ground coverage. The resulting positions are denoted by either an N (near) or F (far). The swath width is 50 km to keep the downlink signal within its allocated bandwidth. All production requests were submitted through a Product Generation System (PGS) interface at the Geo-Informatics and Space Technology Development Agency (GISTDA) Earth observation centre. The data employed in this research were single-look complex (SLC) products, which are preprocessed in CEOS (Committee on Earth Observation Satellites) format.

Downloaded by [anuphao aobpaet] at 17:59 21 January 2013

3. Methods

3.1. PSI technique

PSI techniques take advantage of pixels dominated by a single scatterer to reduce the influence of atmosphere and decorrelation. The first algorithms were developed by Ferretti, Rocca, and Prati (2000) and Ferretti, Prati, and Rocca (2001). Similar processing strategies have been developed by Crosetto et al. (2003), Lyons and Sandwell (2003), Werner et al. (2003), and Kampes (2005). These methods have been very successful for InSAR analysis of radar scenes containing large numbers of man-made structures. One of the limitations of these methods is the PSI selection strategy, which relies heavily on amplitude variation to detect a stable network. These algorithms may fail to detect PSI when the number of images is limited (less than 20) or when the PSI has low amplitude.

In contrast, StaMPS (Hooper, Segall, and Zebker 2007) overcomes this limitation by using the spatially correlated part of the phase measurements to detect a stable network in association with the amplitude. In the first step, we form interferograms with respect to a single 'master' image acquired on 27 July 2008, which was chosen to maximize coherence (see Figure 3(*a*)). The rest of the images are then co-registered to the master image. Once the mapping functions are estimated, each image is resampled to the master geometry using a 12-point raised cosine interpolation kernel, yielding 18 interferograms. An initial selection of candidate pixels based on analysis of amplitude dispersion is performed to reduce computer load. The phase is then analysed to estimate the phase stability of these pixels in an iterative process. For each candidate pixel x in the ith interferogram, the spatially correlated contribution to the phase, $\tilde{\phi}_{x,i}$, is estimated by band-pass filtering the phase of pixels in the neighbourhood and subtracted from the interferometric phase, $\phi_{x,i}$.

The spatially uncorrelated look angle error, $\Delta\hat{\phi}^{u}_{\theta,x,i}$, (often referred to as digital elevation model (DEM) error) is estimated from the residual phase using its correlation with a perpendicular baseline. What remains after subtraction of these two terms is assumed to be phase noise and is used to calculate a coherence-like measure, γ_x, for each pixel,

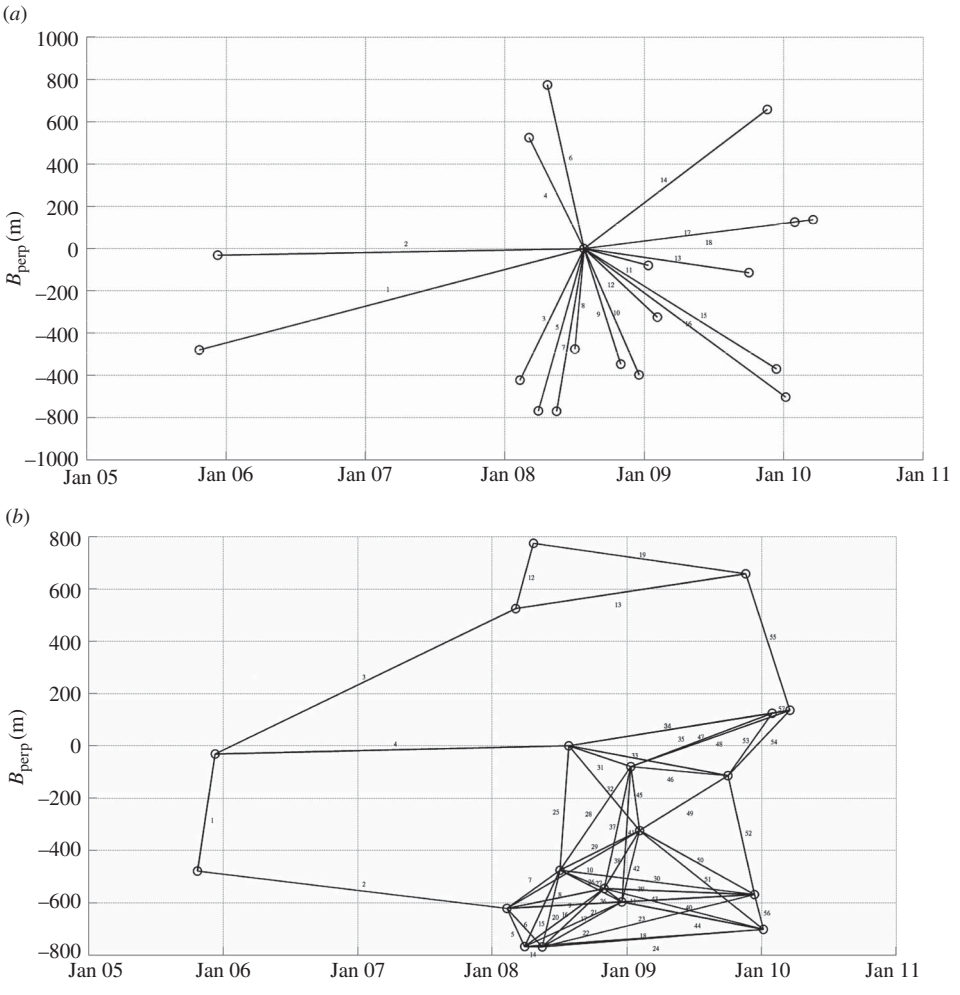

Figure 3. Baseline plots for (*a*) the PSI processing and (*b*) the small baseline processing. In both cases, perpendicular baselines (B_{perp}) are with respect to the master image used in PSI processing. Circles represent images and lines represent the interferograms formed.

$$\gamma_x = \frac{1}{N}\left|\sum_{i=1}^{N}\exp\left\{\sqrt{-1}\left(\phi_{x,i} - \tilde{\phi}_{x,i} - \Delta\hat{\phi}^{u}_{\theta,x,i}\right)\right\}\right|, \tag{1}$$

where N is the number of interferograms. A threshold value for coherence, γ_x, is set based on the acceptable density of false identifications, and pixels with coherence above this threshold value are selected as PSI pixels.

3.2. SB technique

In SB methods (see, e.g. Berardino et al. 2002; Schmidt et al. 2003; Fornaro, Pauciullo, and Serafino 2009), a network of interferogram pairs is created with small temporal and geometrical baselines to limit de-correlation noise. Noise is further reduced by applying

Downloaded by [anuphao aobpaet] at 17:59 21 January 2013

range and azimuth filters (Just et al. 1994) and spatial multilooking. However, filtering reduces spatial resolution, which can result in failure to detect some stable isolated pixels. We use the full-resolution SB method of Hooper (2008), in which pixels are identified among the candidate pixels in essentially the same way as for PSI pixels, based on phase analysis. For SB processing, we form interferograms with an estimated mean coherence above a threshold of 0.3. We also add additional connections to ensure that there are no isolated clusters of images (see Figure 3(*b*)), creating a total of 57 interferograms.

3.3. Combined PSI and SB method

Hooper (2008) proposed a combination of PSI and SB algorithms to take full advantage of both techniques. The combination of the two sets of pixels increases the number of observations with useable signals and also increases the signal-to-noise ratio for pixels selected by both methods. The PSI and SB data sets are combined before phase unwrapping (unfolding the phase out of its natural range of $-\pi$ to π) to maximize the reliability of the unwrapped phase. A combined data set of SB interferograms phase is created from pixels selected by both the PSI and SB methods. A weighted mean value for the phase is calculated when a pixel occurs in both data sets by summing the complex signal from both data sets with the amplitude of each set to an estimate of the signal-to-noise ratio for the pixel in that data set.

The combined observations are then 'unwrapped' using a statistical cost approach (Hooper 2010). After phase unwrapping, spatially correlated DEM errors are estimated from their correlation with perpendicular baseline. The phase is then re-unwrapped by subtracting DEM error, to improve unwrapping accuracy for larger baselines.

4. Results and discussion

We calculate the mean deformation rates from the unwrapped time series using linear least squares. These estimates are relative to the area centred on the benchmark (B52), for easy comparison with levelling. This benchmark is situated in a relatively stable area. To reduce the influence of noise associated with single scatters, we take the average rate of pixels lying at a distance of less than 100 m from B52. We therefore assume that the deformation signal does not change significantly over this distance, which is reasonable for the case of deformation caused by water pumping. We also assume that the scattering mechanism, which mainly depends on the building type and orientation, does not vary over this distance. In order to convert from line-of-sight to vertical, we make the assumption that there is no significant horizontal displacement and determine the vertical deformation rate by simply dividing the line-of-sight displacement by the cosine of the incidence angle. The mean incidence angle of RADARSAT-1 is 38° and the cosine is 0.8. Thus, in this case, the estimated vertical deformation rate is up to ~30.0 mm year^{-1}. Figure 4(*a*) shows the results of this estimation. The average pixel density in the study area is 120 km^2 and over 150 km^2 in the urbanized areas. We also calculate the standard deviations of the mean velocity by the percentile bootstrap method (Efron and Tibshirani 1986). Most of the estimated velocities have standard deviations of less than 1 mm year^{-1}. This means that both atmospheric signal and unwrapping errors have a negligible contribution in the rate estimation; otherwise, it would appear reflected when estimating the precision with bootstrapping. However, there are areas in the southwest and in the eastern part where the standard deviations are up to 6 mm year^{-1} (Figure 4(*b*)). This may be caused by atmospheric artefacts, unwrapping errors, or real deviations of the subsidence in these areas from linear behaviour. The rates obtained for these areas should be regarded with caution.

Downloaded by [anuphao aobpaet] at 17:59 21 January 2013

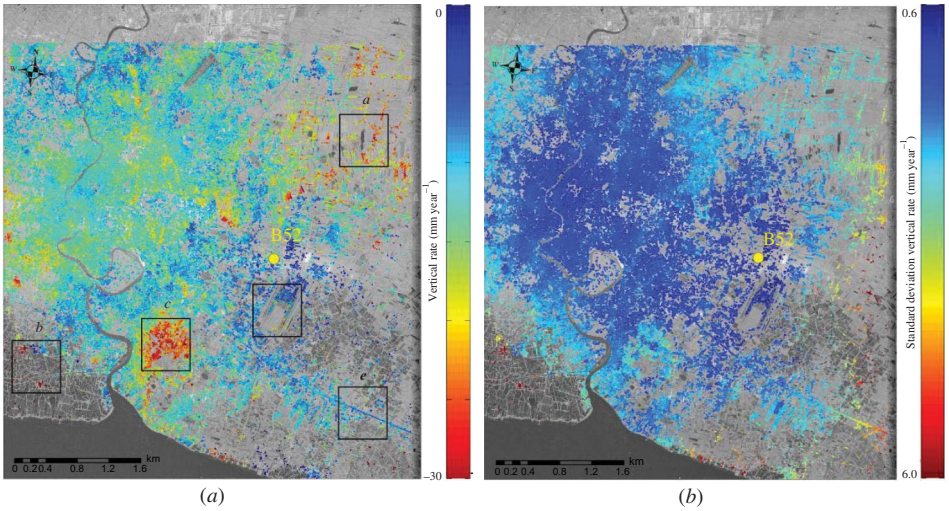

(*a*) (*b*)

Figure 4. (*a*) Subsidence rate (mm year^{-1}) from InSAR time-series analysis and (*b*) standard deviations of mean rates (mm year^{-1}).

To explore the variation of subsidence in the study area, we chose five areas that display different subsidence patterns, the locations are shown in Figure 4(*a*). Figure 5(*a*) shows the agricultural Nongchok district of Bangkok, which includes a lake and paddy fields surrounded by villages. The subsidence rate in the area is between 10 and 30 mm year^{-1} due to the soft clay and over-pumping of ground water for irrigation. This area is set as a critical groundwater pumping zone following the 'Groundwater Act for the Implementation of Groundwater Management Measurement' of the Department of Mineral Resources (Provincial Waterworks Authority 2010). Figure 5(*b*) includes the coastal zone and southern neighbouring provinces (Samut Prakarn and Na Klua) in which severe flooding has occurred, probably caused by a combination of erosion and land subsidence (DMR 2011). For this area, we also find strong subsidence of ~25 mm year^{-1}. These values must be treated with caution as the low density of PSI may have compromised phase unwrapping. The area of Samut Prakarn–Thepharak (Figure 5(*c*)) shows subsidence rates that reflect the rapid development of an urban industrial zone in recent years.

Figure 5(*d*) is located at Suvarnabhumi Airport. Here, we detect the subsidence of the runway at a rate of 20 mm year^{-1}. This contrasts with the slower deformation at the terminal building (0.5 mm year^{-1}), which is built on piles resting on the sand layer. Finally, Figure 5(*e*) shows the difference in land subsidence between the ground surface and the sand layer. The highway in Figure 5(*e*) is built on piles that stand on the sand layer around 21 m beneath the ground surface and appears to be very stable.

5. Validation with levelling

5.1. Mean velocity

We compare the average velocities from InSAR and levelling using B52 as a reference. The mean velocities of all pixels within a 100 m radius of each benchmark are averaged. As explained earlier, we do not expect the deformation caused by groundwater pumping to change significantly over this distance. Table 1 shows the velocity values estimated from both levelling and InSAR using least squares.

Downloaded by [anuphao aobpaet] at 17:59 21 January 2013

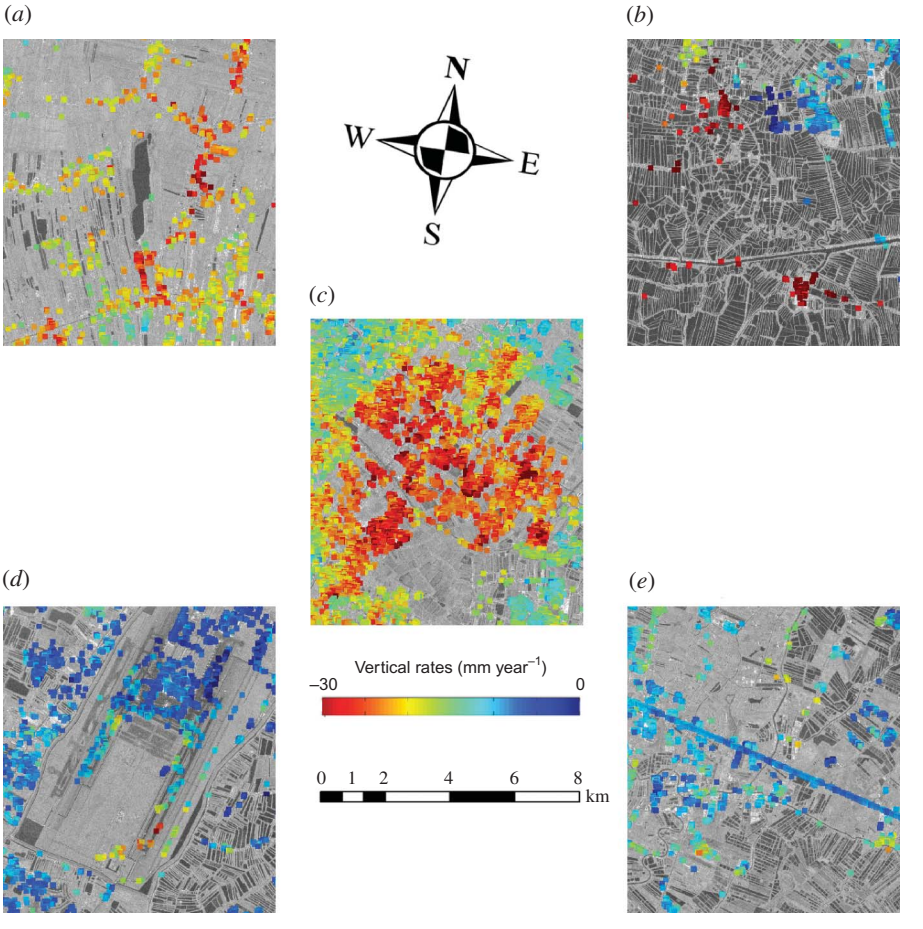

Figure 5. Subsidence rate (mm year^{-1}) plotted on the mean radar amplitude. (*a*) Bangkok–Nongchok, (*b*) Samut Prakarn–Na Klua, (*c*) Samut Prakarn–Thepharak, (*d*) Suvarnabhumi Airport, and (*e*) Bangna–Trad Road.

We compare InSAR against levelling rates (v_{InSAR} and v_{lev}, respectively) using the *t* test, (Fisher 1925),

$$t = \frac{v_{\mathrm{InSAR}} - v_{\mathrm{lev}}}{\sqrt{\sigma^2_{\mathrm{InSAR}} + \sigma^2_{\mathrm{lev}}}}, \tag{2}$$

where the parameter *t* is a double-tailed Student distribution, and $\sigma^2_{\mathrm{InSAR}}$ and σ^2_{lev} are the InSAR and levelling rates variances, respectively. Using a level of confidence of 95%, we find that 80% of the benchmarks agree with the estimation from InSAR. In other words, the distribution of the difference in rates is close to that expected. Nevertheless, we find that for some benchmarks, e.g. B5, B42, and B45, there are significant differences between levelling and InSAR rates. One possible explanation for these differences could be the nature of the scatterers contributing to the InSAR measurements. Ground scatterers (ground to wall reflections) are expected to subside faster than, for example, rooftop scatterers, because buildings usually have deep foundations (see Figure 2). In any case, based on the

Downloaded by [anuphao aobpaet] at 17:59 21 January 2013

Table 1. Comparison of subsidence rates between InSAR and levelling with standard deviation (mm year^{-1}) using B52 as a references.

	InSAR (mm year^{-1})		Levelling (mm year^{-1})			InSAR (mm year^{-1})		Levelling (mm year^{-1})	
Benchmark identifier	Rate	Standard deviation	Rate	Standard deviation	Benchmark identifier	Rate	Standard deviation	Rate	Standard deviation
B1	−2.15	±1.60	−1.67	±1.67	B37	0.06	±1.40	1.15	±0.56
B2	−3.60	±1.49	−4.19	±0.99	B38	−0.54	±1.49	−4.40	±0.94
B3	−0.86	±1.45	−2.90	±0.83	B39	−0.80	±1.56	−7.48	±1.65
B4	−0.55	±1.43	−2.51	±1.54	B40	−2.05	±1.33	−6.40	±1.61
B5	−7.58	±1.80	−0.66	±0.92	B41	−5.73	±1.50	−0.06	±0.60
B6	−2.51	±1.79	1.42	±1.02	B42	−10.12	±1.20	−1.99	±0.81
B7	−8.43	±1.16	−1.58	±0.79	B43	−7.36	±2.08	−0.66	±0.52
B8	2.46	±1.41	−1.46	±0.56	B44	−0.87	±1.33	−1.09	±0.64
B9	−3.03	±1.46	−0.78	±0.89	B45	−6.75	±1.79	−0.62	±0.65
B10	−1.55	±1.54	−3.57	±0.61	B46	−5.95	±1.66	−3.17	±2.30
B11	2.28	±1.18	0.77	±1.18	B47	−0.54	±1.54	1.25	±1.00
B12	−4.47	±1.33	−4.71	±1.20	B48	−3.31	±1.43	−1.61	±1.33
B13	–	–	−1.71	±0.64	B49	–	–	−5.53	±1.07
B14	−2.53	±1.43	−3.46	±1.32	B50	2.43	±1.49	1.80	±0.44
B15	−2.88	±1.45	−4.30	±0.98	B51	−3.24	±1.30	0.71	±0.77
B16	−3.25	±1.42	−2.81	±1.42	B52	0.00	0.00	0.00	0.00
B17	−3.02	±1.50	−2.48	±1.01	B53	3.10	±1.06	1.40	±1.00
B18	−3.74	±1.50	−0.44	±1.29	B54	–	–	1.64	±0.80
B19	−0.17	±1.49	−2.61	±0.61	B55	−3.26	±1.41	−5.05	±0.92
B20	−5.89	±1.60	−1.17	±1.48	B56	−3.56	±1.46	−3.41	±1.01
B21	−0.96	±1.52	−2.52	±1.24	B57	−5.04	±1.38	−3.67	±0.72
B22	−0.96	±1.69	−3.09	±1.12	B58	−3.93	±1.48	−5.10	±1.25
B23	−0.96	±1.64	−1.69	±0.55	B59	−5.23	±1.57	−5.80	±1.11
B24	−1.07	±1.62	−2.39	±0.38	B60	−3.41	±1.56	−3.76	±0.81
B25	−1.98	±1.79	−1.42	±0.80	B61	−2.55	±1.41	−4.72	±0.98
B26	−6.83	±1.60	−6.18	±1.53	B62	−3.51	±1.39	−5.37	±2.03
B27	−1.96	±1.51	−4.78	±1.19	B63	−3.35	±1.44	−5.64	±0.79
B28	−3.86	±1.45	−3.54	±1.05	B64	−4.81	±1.54	−3.44	±0.54
B29	−4.26	±1.50	−4.51	±2.21	B65	−6.46	±1.80	−2.77	±0.84
B30	−4.03	±1.46	−3.52	±1.09	B66	−8.71	±1.51	−3.44	±1.05
B31	−5.14	±1.51	−3.53	±1.16	B67	−1.27	±1.46	−4.14	±1.23
B32	−3.47	±1.66	−5.18	±1.68	B68	−4.08	±1.53	−3.68	±0.68
B33	−4.42	±1.53	−3.22	±2.02	B69	–	–	−4.26	±0.97
B34	−2.15	±1.53	−4.86	±1.20	B70	−3.43	±1.50	−1.82	±0.83
B35	−2.28	±1.51	−4.61	±0.89	B71	–	–	−4.17	±2.43
B36	−3.36	±1.51	−3.49	±0.79					

Note: Negative values indicate subsidence and '–' alone indicates there were no PSI within 100 m of the benchmark.

t test we perform for the rates, it seems that in most of the cases (80%), InSAR pixels seem to relate to infrastructure. However, scatterer characterization is complex to assess and is beyond the scope of this article.

5.2. Time series

For a more detailed analysis, we also compare the time series from InSAR and levelling for selected points. Figure 6 shows the time series of the selected benchmarks for which deformation velocities from both techniques are in agreement. These benchmarks are B14,

Downloaded by [anuphao aobpaet] at 17:59 21 January 2013

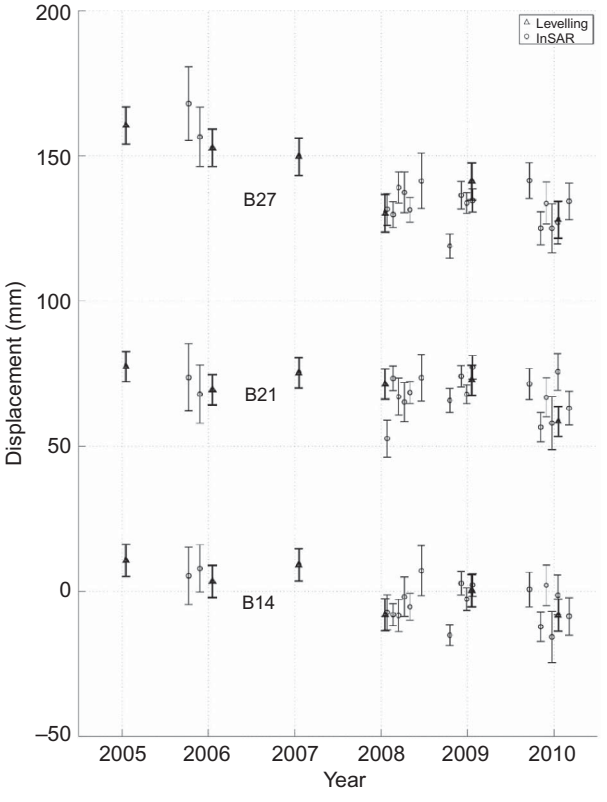

Figure 6. Displacement time series obtained from InSAR and levelling for three benchmarks for which the mean displacement rates are in agreement. Vertical offsets are added for visualization.

B21, and B27 (locations are shown in Figure 9). We find a reasonable agreement between the results of the two data sets. Although the comparison is not entirely straightforward, because InSAR observations are acquired at different times to levelling, the two data sets can be said to agree at the $1-\sigma$ error level.

We also plot one benchmark for which the rates from levelling and InSAR disagree (Figure 7). Although the measured displacements between the two techniques are in general agreement, there are strong nonlinear motions detected by InSAR from 2009 on, which are not visible in the levelling data, perhaps due to the limited temporal sampling. The low number of scatterers near B7 and the potential contribution to the displacement estimates from double-bounce echoes, which express the displacement of the ground rather than the buildings, may be the contributing factors, respectively, leading to noisier estimates and a larger InSAR subsidence rate. Figure 8(*a*) compares the distribution of pixels for B7 with a benchmark (B27), where InSAR and levelling agree. Atmospheric delay also contributes to the noise for the InSAR time series. In fact, atmospheric noise was not subtracted due to the bad temporal sampling of SAR images and the inherent difficulty of separating it from nonlinear motion. Selection of the reference point cannot be the cause of the differences between levelling and InSAR because otherwise all the time series would be affected.

5.3. Comparison of interpolated rates

In the previous subsections, we have shown that the mean rates and temporal pattern of displacement are generally in good agreement between levelling and InSAR. We now explore

Downloaded by [anuphao aobpaet] at 17:59 21 January 2013

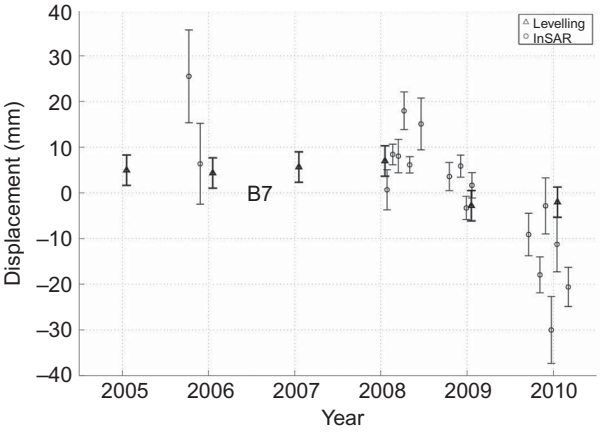

Figure 7. Displacement time series obtained from InSAR and levelling for benchmark B7, for which rates from the two techniques are not in agreement.

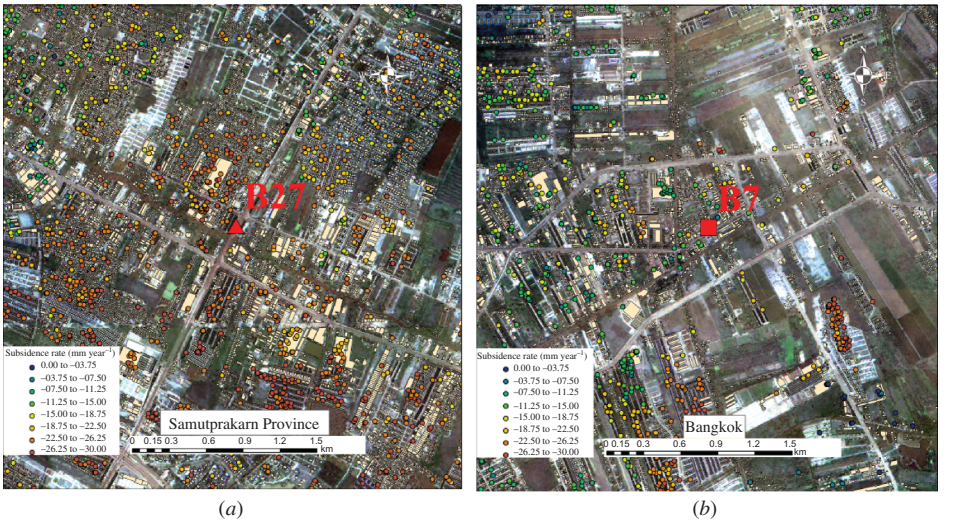

(*a*) (*b*)

Figure 8. Displacement rates in the neighbourhood of two selected levelling benchmarks. (*a*) Benchmark B27 is surrounded by many coherent targets due to the high number of buildings in the vicinity. (*b*) B7 is located in northeast Bangkok, which is a rapidly growing suburban area. Fewer points are within a 100 m radius, which likely contributes to the disagreement between levelling and InSAR for this benchmark.

the spatial pattern of the deformation signal through spatial interpolation. The inverse distance weighted interpolation technique determines cell values using a linearly weighted combination of a set of sample points. It depends on the inverse of the distance raised to a mathematical power, which we set to be 2 (‘inverse square’). Figure 9 shows the spatial pattern of levelling and InSAR after spatial interpolation. In general, the map reveals similar patterns for both InSAR and levelling. We see that InSAR provides a more detailed map due to a larger number of observations. Major differences occur mostly in areas where there is a lack of levelling benchmarks. For example, in the southeast, we detect a subsiding area with InSAR that is not revealed by levelling.

Downloaded by [anuphao aobpaet] at 17:59 21 January 2013

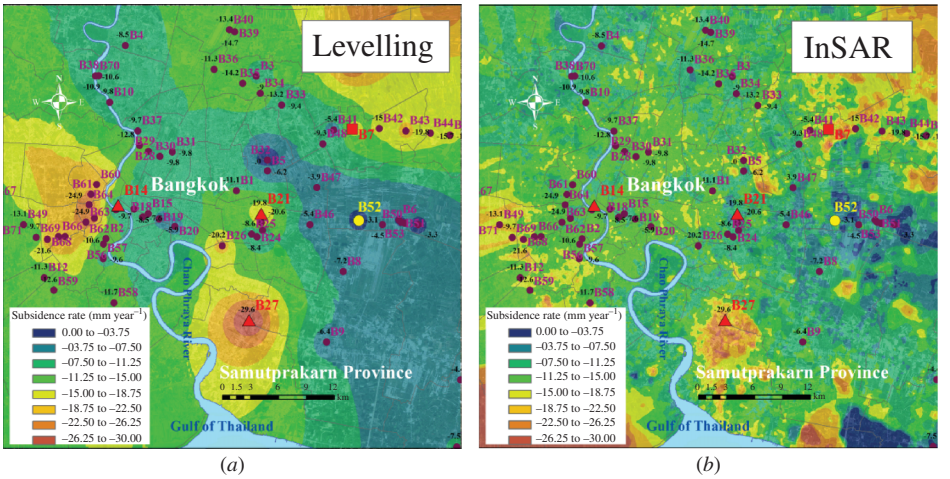

(*a*) (*b*)

Figure 9. Spatial interpolation of subsidence rate (mm year^{-1}) from (*a*) levelling and (*b*) InSAR using inverse distance weighted interpolation. Coloured symbols represent levelling benchmarks, with red triangles indicating the benchmarks shown in Figure 6 and the red square indicating the benchmark shown in Figure 7. The yellow circle indicates the reference benchmark.

6. Conclusions

The application of a multitemporal InSAR approach that combines both PSI and SB methods detected approximately 300,000 pixels that can serve as monitoring points. These observations provide better spatial density by orders of magnitude than levelling. Deformation rates have been estimated for the period 2005–2010, with a maximum relative rate of about 30 mm year^{-1}. Velocities estimated from InSAR agree with those estimated from levelling, within the measurement uncertainty, for 80% of the levelling benchmarks.

In this comparison, we have used all coherent targets at a distance of up to 100 from the benchmarks. Therefore, the high agreement that we have found suggests that the deformation does not change over this distance. From this, we also conclude that most of the scattering objects seem to match the benchmark type. For example, since most of the benchmarks are located on buildings (and infrastructure), the results suggest that most of the scatterers are also located on buildings.

Until now, the principal source of information about vertical ground movements has come from annual levelling campaigns by the RTSD, which have been carried out since 1978. While levelling is a reliable technique, the distribution of points in the levelling network is sparse. On the other hand, the results from InSAR provide a very high observation density. InSAR should, therefore, be considered to be a complementary technique to levelling for monitoring deformation in Bangkok.

Acknowledgements

The research was supported by the European Union GEO2TECDI project. The authors thank the Geo-Image Technology Research Unit, Department of Survey Engineering, and Chulalongkorn University for facilities support. The RADARSAT-1 SAR data used in this work are provided by the Geo-Informatics and Space Technology Development Agency (GISTDA) cooperating with the Canadian Space Agency (CSA) and MacDonald, Dettwiler and Associates Ltd. (MDA). The levelling survey data are provided by Royal Thai Survey Department.

Downloaded by [anuphao aobpaet] at 17:59 21 January 2013

Downloaded by [anuphao aobpaet] at 17:59 21 January 2013

References

Berardino, P., G. Fornaro, R. Lanari, and E. Sansosti. 2002. "A New Algorithm for Surface Deformation Monitoring Based on Small Baseline Differential SAR Interferograms." *IEEE Transactions on Geoscience and Remote Sensing* 40 (11): 2375–2383.

Bontebal, M. 2001. "Land Subsidence in Bangkok." Accessed August 25, 2010. http://www.unescap.org//esd/energy-security-and-water-resources/water/urbangeology/land/index.asp

Brand, E. W., and T. Paveenchana. 1971. "Deep-well Pumping and Subsidence in the Bangkok Area." In *4th Asian Regional Conference on Soil Mechanics and Foundation Engineering*, Vol. 1, 1–7. Bangkok, Thailand: Asian Institute of Technology, July 1971.

Crosetto, M., A. Arnaud, J. Duro, E. Biescas, and M. Agudo. 2003. "Deformation Monitoring Using Remotely Sensed Radar Interferometric Data." In *The 11th FIG Symposium on Deformation Measurements*, Santorini, Italy, May 25–28.

Department of Mineral Resources. 2011. "Status of Coastal Geo-Environment in Thailand." Accessed June 26, 2011. http://www.dmr.go.th/ewtadmin/ewt/dmr_web/main.php?filename=coastal_En

Edward, W. 1976. "Soil Compressibility and Land Subsidence in Bangkok." In *Publication No. 121 of the International Association of Hydrological Sciences, Proceedings of the Anaheim Symposium*, Anaheim, CA, December 13–17.

Efron, B., and R. Tibshirani. 1986. "Bootstrap Methods for Standard Errors, Confidence Intervals, and Other Measures of Statistical Accuracy." *Statistical Science* 1 (1): 54–77.

Ferretti, A., C. Prati, and F. Rocca. 2001. "Permanent Scatterers in SAR Interferometry." *IEEE Transactions on Geosciences and Remote Sensing* 39 (1): 8–20.

Ferretti, A., F. Rocca, and C. Prati. 2000. "Nonlinear Subsidence Rate Estimation Using Permanent Scatterers in Differential SAR Interferometry." *IEEE Transactions on Geoscience and Remote Sensing* 38 (5): 2202–2212.

Fisher, R. A. 1925. "Applications of Student's Distribution." *Metron* 5: 90–104.

Fornaro, G., A. Pauciullo, and F. Serafino. 2009. "Deformation Monitoring Over Large Areas with Multipass Differential SAR Interferometry: A New Approach Based on the Use of Spatial Differences." *International Journal of Remote Sensing* 30 (6, 112): 1455–1478.

Goldstein, R. M., and H. A. Zebker. 1987. "Interferometric Radar Measurement of Ocean Surface Currents." *Nature* 328 (6132): 707–709.

Haley and Aldrich. 1970. *Effect of Deep Well Pumping on Land Subsidence in Bangkok, Part of "Master Plan, Water Supply and Distribution, Metropolitan Bangkok, Thailand"*, Vol. 4. Bangkok: Metropolitan Water Works Association.

Hanssen, R. F. 2001. *Radar Interferometry: Data Interpretation and Error Analysis*, 308 p. Dordrecht: Kluwer Academic.

Hooper, A. 2008. "A Multi-Temporal InSAR Method Incorporating Both Persistent Scatterer and Small Baseline Approaches." *Geophysical Research Letters* 35 (L16302): 5. doi:10.1029/2008GL034654.

Hooper, A. 2010. "A Statistical-Cost Approach to Unwrapping the Phase of InSAR Time Series." In *The FRINGE Workshop 09*, ESA-ESRIN, Frascati (Rome), Italy, November 30–December 4, 2009.

Hooper, A., P. Segall, and H. Zebker. 2007. "Persistent Scatterer Interferometric Synthetic Aperture Radar for Crustal Deformation Analysis, with Application to Volcáno Alcedo." *Journal of Geophysical Research* 112: B07407. doi:10.1029/2006JB004763.

Just, D., and R. Bamler. 1994. "Phase Statistics of Interferograms with Applications to Synthetic-Aperture Radar." *Applied Optics* 33 (20): 4361–4368.

Kampes, B. M. 2005. "Displacement Parameter Estimation Using Permanent Scatterer Interferometry." PhD thesis, Delft University of Technology, The Netherlands.

Kuehn, F., A. Margane, T. Tatong, and T. Wever. 2004. "SAR-Based Land Subsidence Map for Bangkok, Thailand." *Zeitschrift für Angewandte Geologie* 50: 74–81.

Lyons, S., and D. Sandwell. 2003. "Fault Creep along the Southern San Andreas from Interferometric Synthetic Aperture Radar, Permanent Scatterers, and Stacking." *Journal of Geophysical Research* 108 (B1): 2047–2070.

Marinkovic, P., G. Ketelaar, F. van Leijen, and R. Hanssen. 2008. "In-SAR Quality Control: Analysis of Five Years of Corner Reflector Time Series." In *Fifth International Workshop on ERS/Envisat SAR Interferometry, 'FRINGE07'*, Frascati, Italy, November 26–30, 2007.

Nutalaya, P. 1981. *Investigation of Land Subsidence Caused by Deep Well Pumping in the Bangkok Area*. Comprehensive Report 1978–1981, Submitted to National Environmental Board, Asian Institute of Technology, Bangkok.

Perissin, D. 2008. "Validation of the Submetric Accuracy of Vertical Positioning of PSs in C-Band." *IEEE Transactions on Geosciences and Remote Sensing Letters* 5 (3): 502–506.

Phien-wej, N., P. H. Giao, and P. Nutalaya. 2006. "Land Subsidence in Bangkok, Thailand." *Engineering Geology* 82: 187–201.

Provincial Waterworks Authority. 2010. "Critical Groundwater (Thai Language)." Accessed December 8, 2010. http://www.pwa.co.th/document/deepwell.html

Ramnarong, V. 1983. "Groundwater Depletion and Land Subsidence in Bangkok." In *Proceedings of Conference on Geology and Mineral Resources of Thailand*. Department of Mineral Resources, Bangkok, Thailand, November 19–28.

Ramnarong, V., S. Buapeng, S. Chootnatut, and A. Loupensri. 1998. *Groundwater and Land Subsidence Crisis in Bangkok Metropolitan and Vicinity*, Vol. 3. Technical Report of Department of Mineral Resources, Bangkok, Thailand.

Schmidt, D. A., and R. Burgmann. 2003. "Time-Dependent Land Uplift and Subsidence in the Santa Clara Valley, California, from a Large Interferometric Synthetic Aperture Radar Data Set." *Journal of Geophysical Research* 108 (B9): 2416–2428.

Werner, C., U. Wegmuller, T. Strozzi, and A. Wiesmann. 2003. "Interferometric Point Target Analysis for Deformation Mapping." In *International Geoscience and Remote Sensing Symposium (IGARSS)*, Toulouse, France, July 21–25.

Worawattanamateekul, J. 2006. "The Application of Advanced Interferometric Radar Analysis for Monitoring Ground Subsidence: A Case Study in Bangkok." PhD thesis, Technical University of Munich, Germany, 169 p.

Yong, R. N., H. Maathuis, and E. Turcott. 1995. "Groundwater Abstraction-Induced Land Subsidence Prediction: Bangkok and Jakarta Case Studies." In *The Fifth International Symposium on Land Subsidence, FISOLS-95*, The Hague, The Netherlands, October 16–20.

Downloaded by [anuphao aobpaet] at 17:59 21 January 2013